

# Supplemental Material: Atmospheric transport structures shaping the “Godzilla” dust plume

## S1: LCS and FTLE Ridges

In this section we go into detail about how to compute hyperbolic LCS and FTLE ridges. Then, the conditions which guarantee that a FTLE ridge is a hyperbolic FTLE are covered. Finally, we briefly summarize the benefits and drawbacks of each to allow the reader to decide what is best to use for their application.

### LCS

We begin by detailing the conditions which guarantee a material line is a hyperbolic LCS. In this section, we are mainly summarizing parts of the theory laid out in [1] and the computational aspects presented in [2]. For more detail, we refer the readers to the mentioned papers. From [2], we present the relaxation of Theorem 1 but use the eigenvalue/vector ordering consistent with our paper ( $\lambda_1 \geq \lambda_2$ ). Given we have a sufficiently smooth dynamical system defined over a 2-dimensional domain  $U$  and a corresponding family of flow maps (as in the main text), the right Cauchy-Green strain tensor is given by,

$$\mathbf{C}_{t_0}^{t_0+T}(\mathbf{x}_0) = (\nabla \mathbf{F}_{t_0}^{t_0+T})^\top \nabla \mathbf{F}_{t_0}^{t_0+T}(\mathbf{x}_0). \quad (1)$$

with real eigenvalues  $\lambda_1, \lambda_2$  and corresponding orthonormal eigenvectors  $\xi_1, \xi_2$  such that,

$$\lambda_1 \geq \lambda_2 > 0 \text{ and,} \quad (2)$$

$$\langle \xi_i, \xi_j \rangle = \delta_{ij}. \quad (3)$$

Given a compact material line  $\mathcal{M}(t) \in U$  which evolves over the interval  $[t_0, t_0 + T]$ ,  $\mathcal{M}(t)$  is a repelling (or attracting if  $T < 0$ ) LCS if and only if the following conditions hold for all initial conditions  $\mathbf{x}_0 \in \mathcal{M}(t_0)$ :

- (A)  $\lambda_2(\mathbf{x}_0) \neq \lambda_1(\mathbf{x}_0) > 1$ ;
- (B)  $\langle \xi_1(\mathbf{x}_0), \nabla^2 \lambda_1(\mathbf{x}_0) \xi_1(\mathbf{x}_0) \rangle \leq 0$ ;
- (C)  $\xi_2(\mathbf{x}_0) \parallel \mathcal{M}(t_0)$ ;
- (D)  $\bar{\lambda}_1(\gamma)$ , the average of  $\lambda_1$  over a curve  $\gamma$ , is maximal on  $\mathcal{M}(t_0)$  among all nearby curves  $\gamma$  satisfying  $\gamma \parallel \xi_2(\mathbf{x}_0)$

(Note:  $\mathcal{M}(t)$  should not be confused with the  $\mathcal{M}$  used in the main text to refer to the underlying manifold over which the domain is defined. Here,  $\mathcal{M}(t)$  refers to a material line within the flow.) Condition (A) makes sure that at a given point along the material line, the normal repulsion/tangential shear ratio is dominated by the normal repulsion and guarantees that the point is not a degenerate point (a point where  $\lambda_1 = \lambda_2$ , leading to ill-defined eigenvector directions). Condition (B) ensures that a point on the curve is at a local maxima of the  $\lambda_1$  field (and therefore of the FTLE field) relative to points in the  $\xi_1$  (perpendicular) direction, and

(C) confirms that the curve is normally repelling (recall  $\xi_1 \perp \xi_2$ ). Finally, (D) is used to pick out the strongest and most influential curves relative to nearby curves satisfying the preceding conditions. To identify these curves in a numerical context, the ODE given by:

$$\mathbf{r}' = \xi_2, \quad |\xi_2(\mathbf{r})| = 1 \quad (4)$$

can be solved while checking at every step that conditions (A) and (B) are satisfied. Doing this produces solution curves (known as shrinklines in this case) which are candidate LCS curves. The true LCS are then found by applying condition (D). There are a number of numerical difficulties that arise as detailed by Farazmand and Haller. To start, while the eigenvalues can be accurately calculated with a relatively coarse spacing used in the finite differences (i.e. the grid size), the eigenvector directions can be extremely sensitive to this spacing. To get around this problem, an auxiliary grid is used around each grid point, with very small spacing, to obtain more accurate eigenvector directions. Though as pointed out by Lekien and Ross [3], using this auxiliary grid for computing the eigenvalues can significantly underestimate the amount of stretching due to the fact that all points of an auxiliary grid will typically be on one side of a LCS due to the small spacing. For this reason, typically eigenvectors will be computed from the auxiliary grid and eigenvalues will be computed from the main grid. Another issue arising from the eigenvector field is that orientation discontinuities will exist and generally can not be rectified globally. This arises because eigenvectors are not uniquely defined (if  $\xi_i$  is an eigenvector, so is  $-\xi_i$ ) and they often can not be globally oriented. To overcome this, eigenvectors can be locally oriented *in place* as (4) is solved (i.e. at each intermediate stage in the ODE solver, the point is checked to make sure the eigenvector direction is consistent with previous steps and rectified if needed). Finally, degenerate points will be present in the eigenvector field. These are points where  $\lambda_1 = \lambda_2$  and the eigenvector direction becomes ill-defined (because the tensor becomes the identity here and every direction is an eigenvector). Farazmand and Haller suggest a re-scaling of (4) where the re-scaling is given by:

$$\alpha(\mathbf{x}_0) = \left( \frac{\lambda_1(\mathbf{x}_0) - \lambda_2(\mathbf{x}_0)}{\lambda_1(\mathbf{x}_0) + \lambda_2(\mathbf{x}_0)} \right)^2. \quad (5)$$

This turns the degenerate points into fixed points of the vector field and therefore solution curves will terminate as they approach these points. For more details on the implementation and helpful visuals we encourage the reader to refer to their paper [2].

## FTLE ridges

A potential drawback of FTLE is that regions of high shear can produce high FTLE and one may mistake a material line along a FTLE ridge for a hyperbolic LCS. A computation performed on ridge points can guarantee a FTLE ridge is in fact a hyperbolic LCS when certain conditions are met [1], though the extraction of the ridge and application of this criteria can sometimes be difficult in a numerical setting due to sensitivity to the underlying grid size (ridges will rarely perfectly align with grid points and accurate eigenvectors of  $\mathbf{C}$  are needed). There are a number of ways around this [4, 5, 6, 7], though all require some extra effort, none are particularly efficient if accurate ridges are desired, and not all are created “equal” (more details below). The simplest way to identify dominant regions is to threshold the FTLE field and focus only on regions above a certain FTLE value. Doing this will identify important regions (not codimension-1 surfaces, though they often encapsulate the true ridges) that have a great deal of influence on the flow. This method is simple and fast making it useful for on the fly applications but one must be aware of potential pitfalls as a region of high shear may be identified instead of attraction/repulsion if one does not apply LCS-FTLE ridge criteria or finds LCS by way of the variational method. In practice, this method is often sufficient as we will demonstrate but

that is not to say there are no exceptions as FTLE ridges can correspond to high shear near centers of vortices or near strong jets.

As mentioned, there are a number of ways to find FTLE ridges [4, 5, 6, 7] but a certain definition allows one to confirm these ridges are LCS in a relatively straightforward manner. Given we have a system detailed above resulting in equations (1) – (3) and a material line  $\mathcal{M}(t_0)$  (in 2D). If the following conditions hold for all  $\mathbf{x}_0 \in \mathcal{M}(t_0)$ :

$$\nabla \lambda_1(\mathbf{x}_0) \in T_{\mathbf{x}_0} \mathcal{M}(t_0), \quad (6)$$

$$\langle \xi_1(\mathbf{x}_0), \nabla^2 \lambda_1(\mathbf{x}_0) \xi_1(\mathbf{x}_0) \rangle < 0 \quad (7)$$

then  $\mathcal{M}(t_0)$  is said to be a FTLE ridge [1]. An equivalent definition is given in [7] and they are referred to as ‘‘C-Ridges’’ there. If ridges are obtained in this manner, Haller [1] gave necessary and sufficient conditions for a FTLE ridge to be a LCS and later, Karrasch [8] simplified these criteria in the case of differentiable eigenvectors, showing that, if  $\mathcal{M}(t_0)$  is a FTLE ridge, then if conditions (A) and (C) from the earlier presented Theorem 1 from [2] hold,  $\mathcal{M}(t_0)$  is a hyperbolic LCS. It should be noted that while this method will guarantee that a FTLE ridge is a LCS, it will not necessarily find *all* LCS as not all LCS are along FTLE ridges [1].

## Numerical Comparisons

We will now briefly summarize the numerical challenges/costs of the LCS computation compared to what is needed for the FTLE. LCS requires at least 5 times the particle integration (due to the auxiliary grid needed for accurate eigenvectors), double the eigenvalue problems need to be solved (since eigenvectors are computed from the auxiliary grid while eigenvalues are computed from the main grid), and further ODE solving needs to be performed to obtain the candidate LCS curves (requiring a custom solver which checks for discontinuities in the eigenvector fields and rectifies them if found along with  $\alpha$  scaling). On top of this, there are many parameters that need to be tuned to obtain satisfactory LCS. That being said, once the parameters are set for a system they should work for general time windows within that system. FTLE on the other hand requires only the initial particle integration, on the main grid, and one eigenvalue problem per grid point. From there thresholding can be applied to obtain dominant FTLE regions. If true ridges are desired, additional work will need to be done to extract those ridges and it is arguably a toss up if FTLE ridge extraction or the variational LCS method is more advantageous; this will be up to the user. Generally, an FTLE ridge approach will be more computationally efficient but at the cost of obtaining less precise (and possibly fewer) structures. In short, computing FTLE and thresholding is the simpler approach, but there is the possibility of obtaining structures which are not truly hyperbolic. In practice, very often *most* structures picked up by the FTLE field are hyperbolic but it is good to be aware of this potential error. That being said, when the analysis is time-sensitive, the FTLE approach is a good choice as it is computationally cheap and simpler to implement. Conversely, finding true LCS gives the precise structures of interest and this can be useful in an analysis context, after the fact, when computation time is of less concern. In addition, it allows one to compute quantities normal and tangent to the ridge. It is no doubt more challenging to implement, but once it is up and running it should be straightforward to use although there will most likely be some knob turning needed when switching between systems.

## S2: Implications of Column-averaged velocity fields

In the text, we mainly focus on FTLE fields derived from column-averaged velocity fields. These velocity fields are averaged from pressure surfaces between 500 hPa - 800 hPa. This is done for

a number of reasons. The main reason we do this is because we are comparing with column-averaged aerosol index data and wanted to make an attempt to capture the influence of the wind at all levels at which dust was present. An additional reason we do this is because, most of these pressure surfaces intersect with the ground at some point and velocity data is not provided where this happens. While these regions were often not in the area we were focused on, we were performing particle integrations starting from a grid within the region we are focused on and therefore, these particle paths sometimes enter these regions of ground interference. Using the averaged velocity field allows us to have a velocity field that is defined all over the globe since averaging at a given point only includes those levels for which we have data. Alternatively, when using a single pressure surface with missing data, one is forced to find some way to deal with these areas. Since there is ground interference we just set the velocity to 0 at these points so when particles enter this area they stop right where they enter. This is what we did for the 600 hPa pressure surface and it resulted in some artificial looking areas because of it.

By performing this averaging, we are no longer solving our system over a well defined manifold. This is in some sense a mathematical formality and can be avoided by imposing a manifold over which our new vector field is defined (say at the average pressure of pressure surfaces used, 650 hPa). In addition, since we are using velocity fields from the atmosphere on a pressure surface, they are essentially incompressible and are treated as such. It is possible to introduce non-negligible compressibility into our averaged vector field by way of the averaging. We checked for this and found that the average divergence over all grid points and all times used in our calculations was  $4.60 \times 10^{-8} \text{ s}^{-1}$  for the averaged fields and  $-2.01 \times 10^{-8} \text{ s}^{-1}$  for a single pressure surface (600h Pa). The maximum divergence (in magnitude) over all grid points and times was  $2.90 \times 10^{-4} \text{ s}^{-1}$  for the averaged fields and  $4.90 \times 10^{-4} \text{ s}^{-1}$  for the 600 hPa velocity fields. Therefore, we conclude that the averaged fields are roughly as compressible as a single pressure surface and this amount is insignificant. While all these concerns could be quelled in our case, it is wise to check these things if taking an approach like this.

### S3: Integration Time

As mentioned, the integration time chosen should be tied to some characteristic time scale of the transport. We settled on approximately half the time it took for the plume to traverse the Atlantic (i.e., half of  $\sim 8$  days) as we were interested in structures that influenced the transport of the plume on this time scale. Often, there is more than one integration time that can be chosen that yields satisfactory results. In Figure 1 below, we show the effect of integration time on the resulting FTLE field. In general, as can be seen in the figure, shorter integration time magnitudes  $|T|$  reveal an FTLE field that is broader, with fewer—and shorter—ridges. In fact, the FTLE field shows “instantaneous” structure in the  $|T| \rightarrow 0$  limit, as discussed in [9], which give the short-time attracting ( $T \rightarrow 0^-$ ) or repelling ( $T \rightarrow 0^+$ ) structures. As the integration time magnitude  $|T|$  is increased, the FTLE field is sharper, with more—and longer—ridges. For our application, picking a shorter time such as  $T = -1$ , or  $-2$  days ((a) and (b) from Figure 1) could potentially miss important structures and produce less well-defined ridges. Choosing a much longer time such as  $T = -5$ ,  $-6$ ,  $-7$ , or  $-8$  days ((e), (f), (g), and (h) from Figure 1) results in an overly complicated FTLE field. Choosing an integration time of  $T = -3$  or  $-4$  days ((c) and (d) from Figure 1) yields results that capture all structures of importance while not being overly complicated. Picking  $T = -3$  days would have been reasonable for the entirety of this paper and in some applications, choosing between candidate integration times comes down to user decision when a single time is not obvious. One could argue that choosing a shorter time is advantageous as this results in a cheaper computation, yet at the risk of missing out on potentially important small scale features. This computational advantage continues when performing ridge or LCS extraction, as shorter integration times result in fewer ridges.

2020-06-17

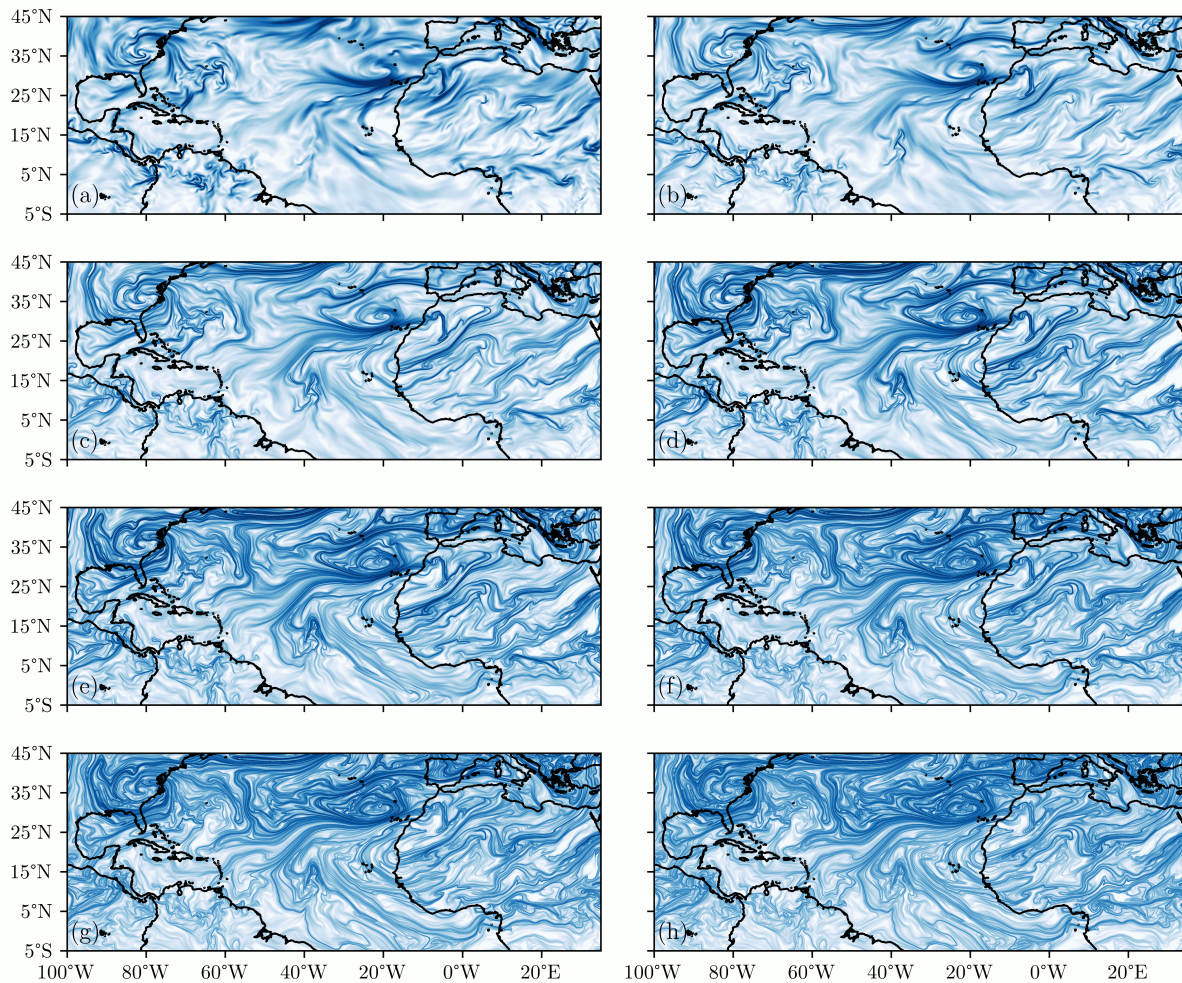


Figure 1: Backward FTLE field from column-averaged velocity fields on June 17, 2020 for integration times  $T =$  (a) -1 day, (b) -2 days, (c) -3 days, (d) -4 days, (e) -5 days, (f) -6 days, (g) -7 days, (h) -8 days,

#### S4: 600 hPa

In this section, we provide figures that were used in the analysis of the dust storm from the 3.1 (FTLE) and 3.2 (Eulerian Combined with Lagrangian Analysis - Early June and Mid June Vortex Comparison) sections of the main text but instead with all of the calculations and comparisons performed on a single pressure surface (600 hPa) instead of the averaged vector field we mainly focused on. No further analysis is presented as the same conclusions are drawn regardless of which underlying vector field was used.

### 3.1 - FTLE

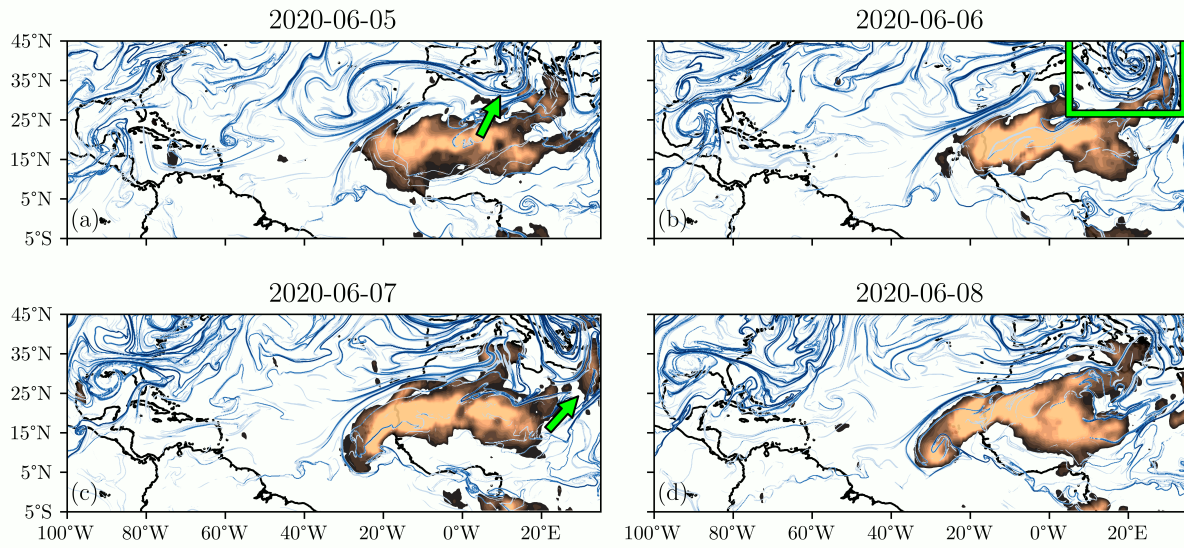


Figure 2: Backward FTLE ridges overlaid on aerosol index data obtained from OMPS, June 5-8, 2020. See text for details.

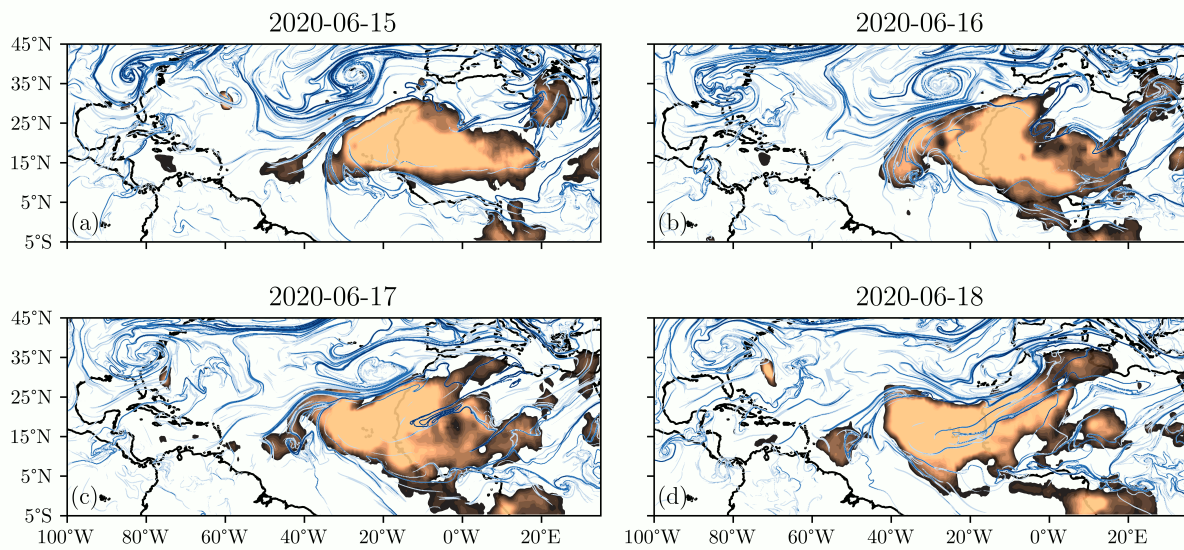


Figure 3: Backward FTLE ridges overlaid on aerosol index data obtained from OMPS, June 15-18, 2020.

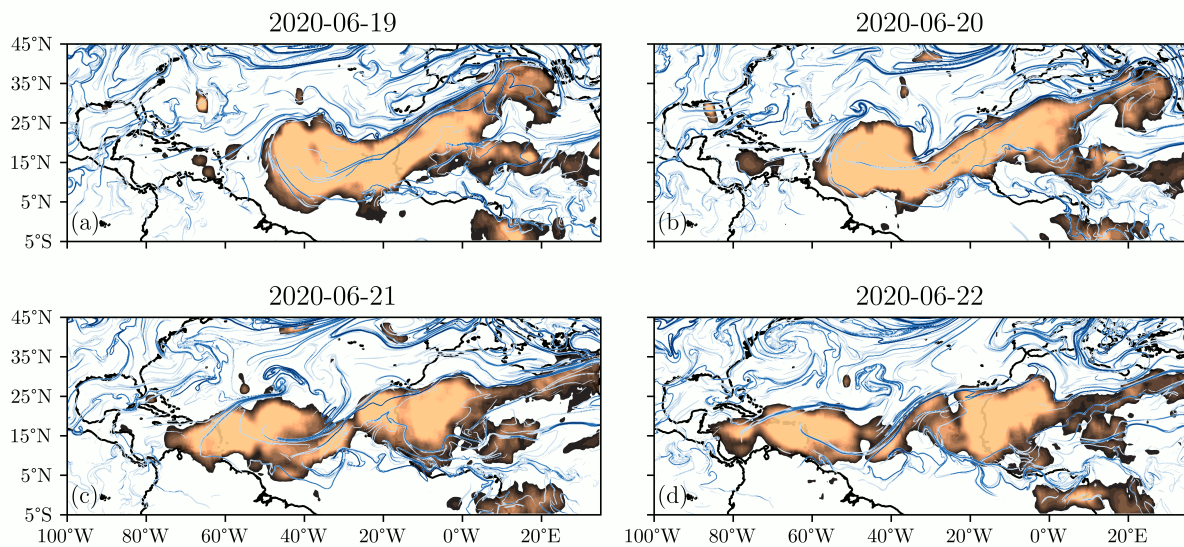


Figure 4: Backward FTLE ridges overlaid on aerosol index data obtained from OMPS, June 19-22, 2020.

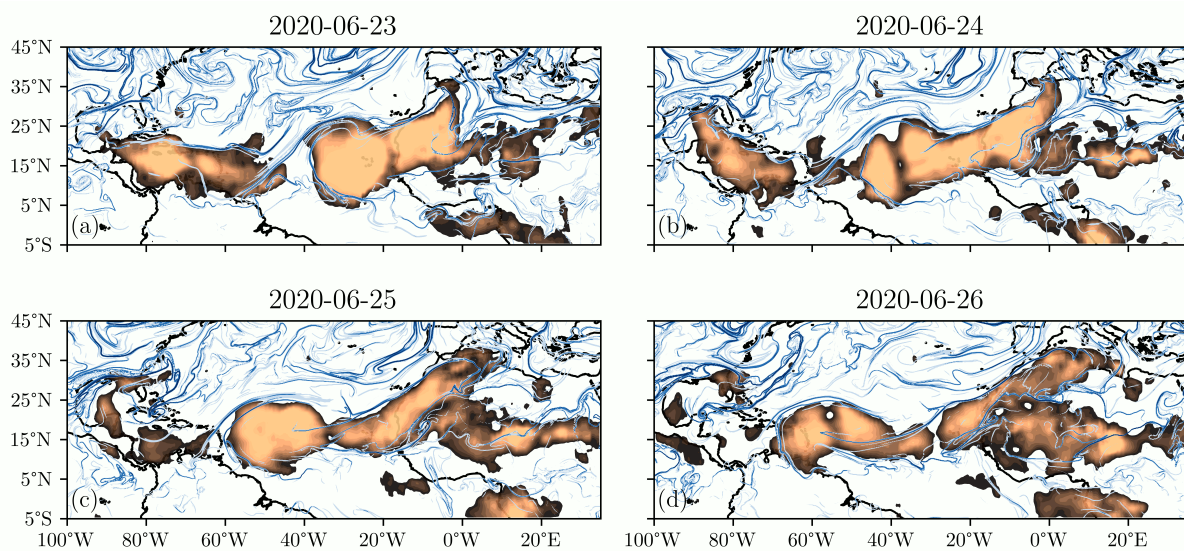


Figure 5: Backward FTLE ridges overlaid on aerosol index data obtained from OMPS, June 23-26, 2020.

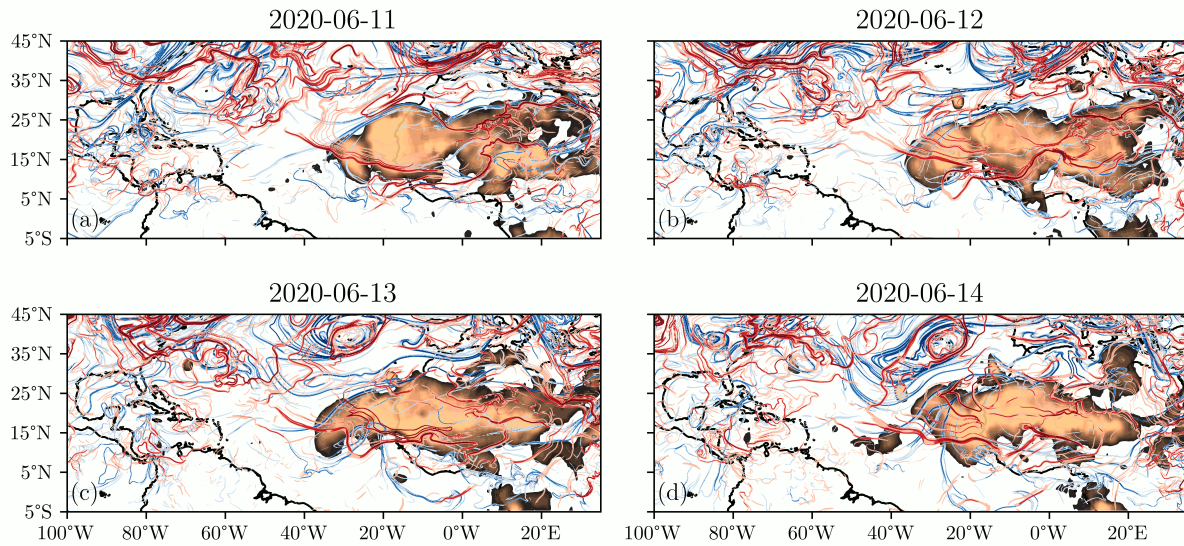


Figure 6: Forward and Backward FTLE ridges overlaid on aerosol index data obtained from OMPS, June 11-14, 2020.

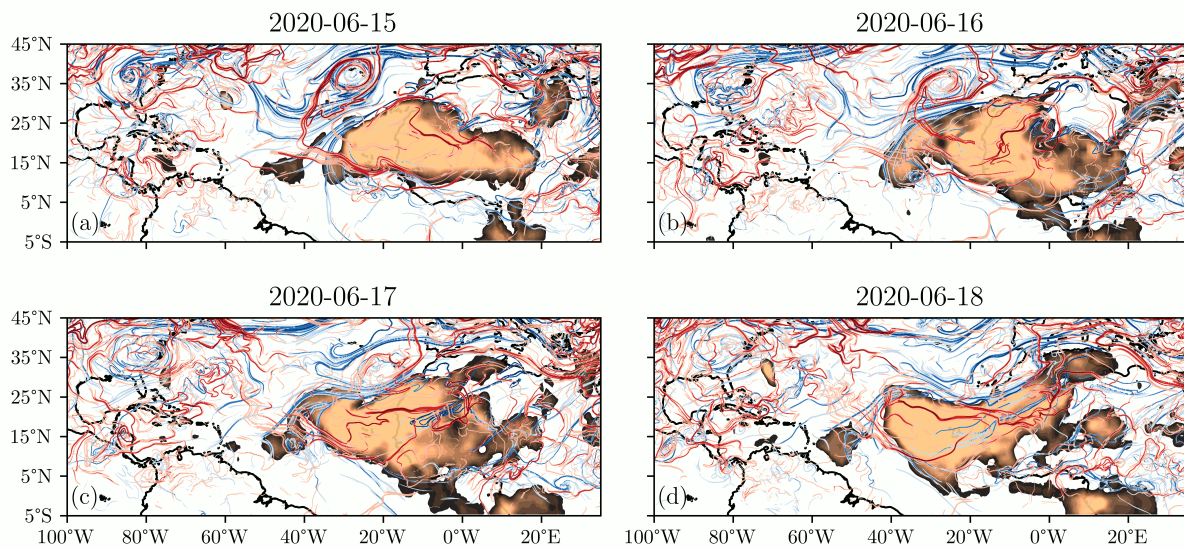


Figure 7: Forward and Backward FTLE ridges overlaid on aerosol index data obtained from OMPS, June 15-18, 2020.

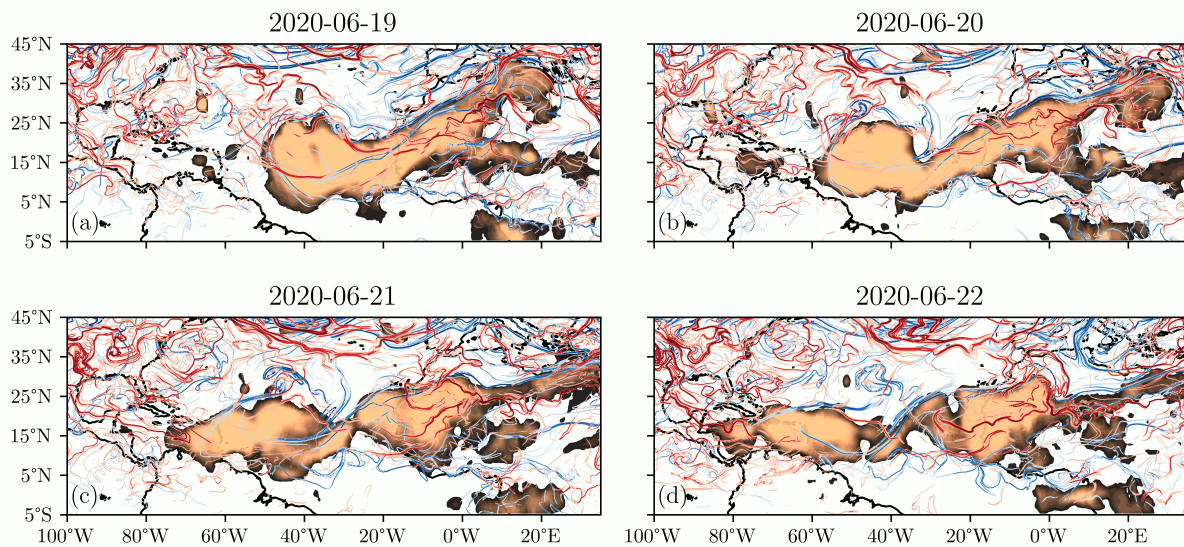


Figure 8: Forward and Backward FTLE ridges overlaid on aerosol index data obtained from OMPS, June 19-22, 2020. See text for details.

### 3.2 - Eulerian Combined with Lagrangian Analysis Early June and Mid June Vortex Comparison

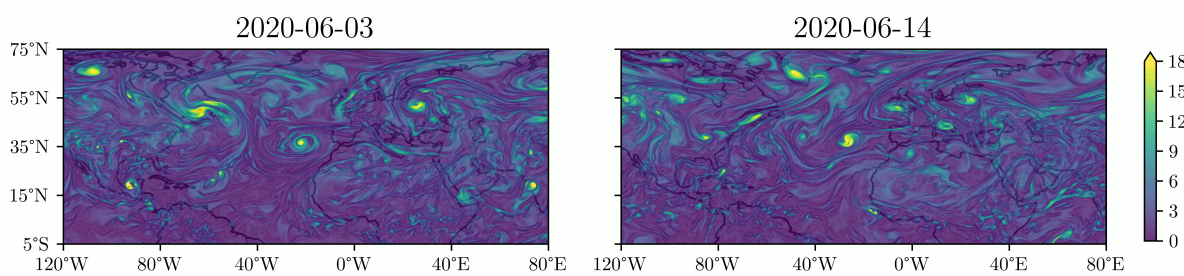


Figure 9: Backward LAVD ( $10^{-5} \times s^{-1}$ , integration time = 1 day) on June 3, 2020 (left) and June 14, 2020 (right).

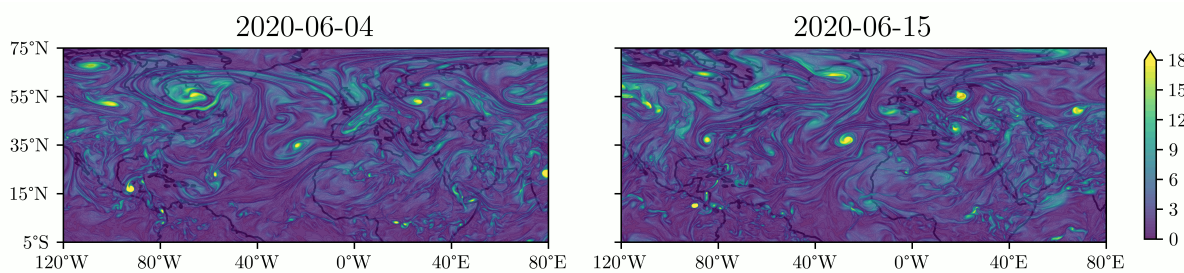


Figure 10: Backward LAVD ( $10^{-5} \times s^{-1}$ , integration time = 1 day) on June 4, 2020 (left) and June 15, 2020 (right).

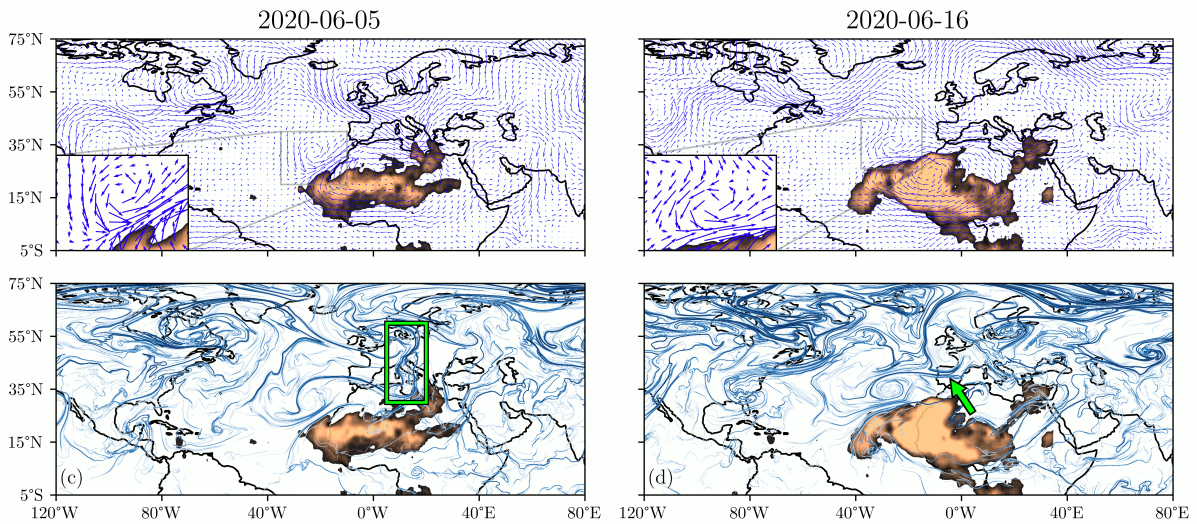


Figure 11: Velocity field (top) and backward FTLE ridges (bottom) overlaid on OMPS aerosol index data on June 5, 2020 (left) and June 16, 2020 (right). See text for details.

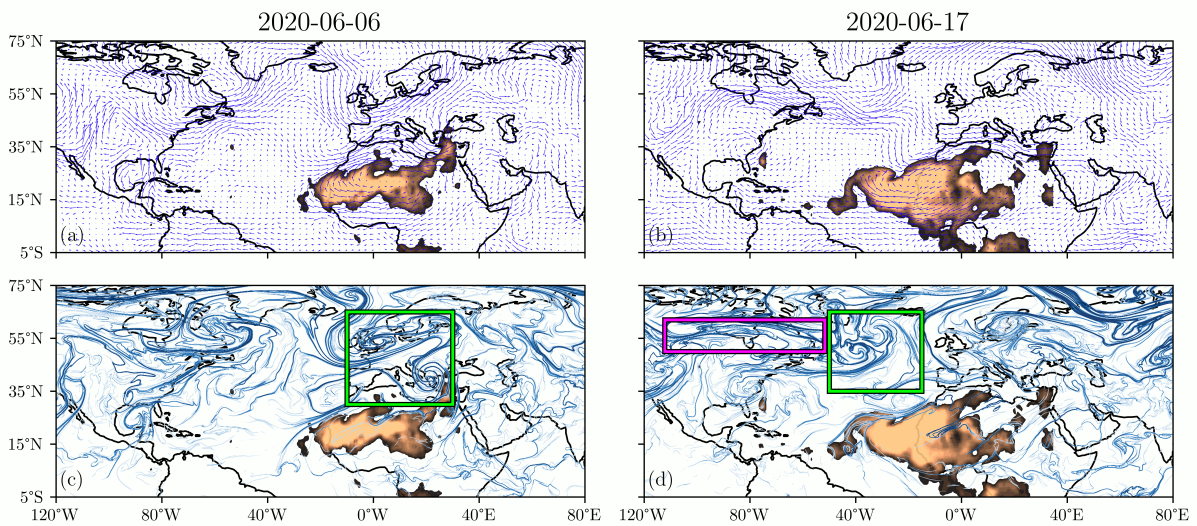


Figure 12: Velocity field (top) and backward FTLE ridges (bottom) overlaid on OMPS aerosol index data on June 6, 2020 (left) and June 17, 2020 (right). See text for details.

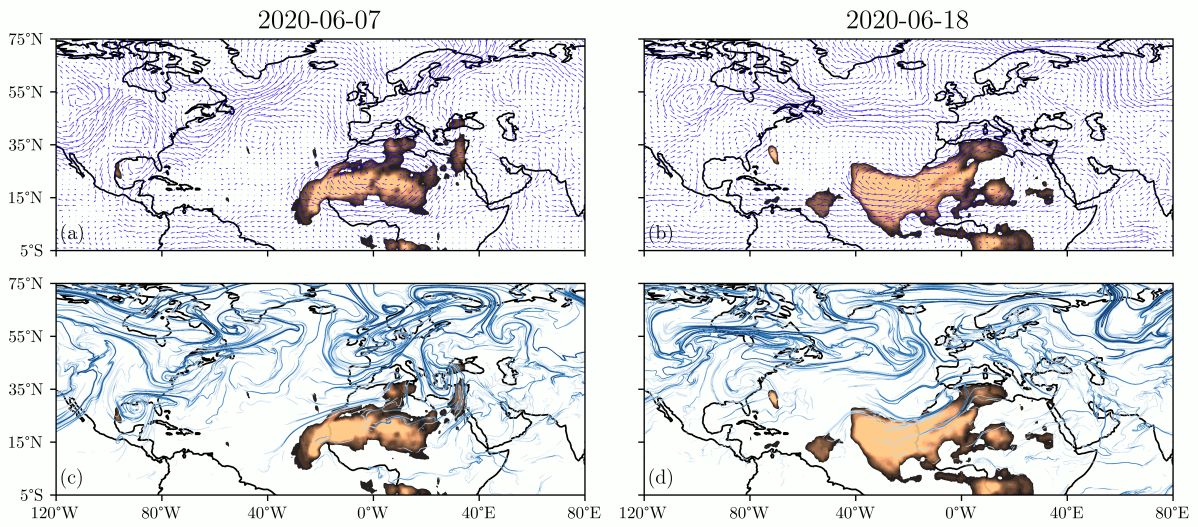


Figure 13: Velocity field (top) and backward FTLE ridges (bottom) overlaid on OMPS aerosol index data on June 7, 2020 (left) and June 18, 2020 (right).

## References

- [1] G. Haller. “A variational theory of hyperbolic Lagrangian coherent structures”. In: *Physica D* 240 (2011), pp. 574–598.
- [2] M. Farazmand and G. Haller. “Computing Lagrangian coherent structures from their variational theory”. In: *Chaos: An Interdisciplinary Journal of Nonlinear Science* 22.1 (Mar. 2012), p. 013128. ISSN: 1054-1500. DOI: [10.1063/1.3690153](https://doi.org/10.1063/1.3690153). eprint: [https://pubs.aip.org/aip/cha/article-pdf/doi/10.1063/1.3690153/16715890/013128\>\\_1\\\_online.pdf](https://pubs.aip.org/aip/cha/article-pdf/doi/10.1063/1.3690153/16715890/013128\>_1\_online.pdf). URL: <https://doi.org/10.1063/1.3690153>.
- [3] F. Lekien and S. D. Ross. “The computation of finite-time Lyapunov exponents on unstructured meshes and for non-Euclidean manifolds”. In: *Chaos* 20 (2010), p. 017505.
- [4] S. C. Shadden, F. Lekien, and J. E. Marsden. “Definition and properties of Lagrangian coherent structures: mixing and transport in two-dimensional aperiodic flows”. In: *Physica D* 212 (2005), pp. 271–304.
- [5] M. Mathur, G. Haller, T. Peacock, J. E. Ruppert-Felsot, and H. L. Swinney. “Uncovering the Lagrangian skeleton of turbulence”. In: *Physical Review Letters* 98 (2007), p. 144502.
- [6] C. Senatore and S. D. Ross. “Detection and characterization of transport barriers in complex flows via ridge extraction of the finite time Lyapunov exponent field”. In: *International Journal for Numerical Methods in Engineering* 86 (2011), pp. 1163–1174. DOI: [10.1002/nme.3101](https://doi.org/10.1002/nme.3101).
- [7] B. Schindler, R. Peikert, R. Fuchs, and H. Theisel. “Ridge Concepts for the Visualization of Lagrangian Coherent Structures”. In: *Topological Methods in Data Analysis and Visualization II: Theory, Algorithms, and Applications*. Ed. by R. Peikert, H. Hauser, H. Carr, and R. Fuchs. Berlin, Heidelberg: Springer Berlin Heidelberg, 2012, pp. 221–235. ISBN: 978-3-642-23175-9. DOI: [10.1007/978-3-642-23175-9\\_15](https://doi.org/10.1007/978-3-642-23175-9_15). URL: [https://doi.org/10.1007/978-3-642-23175-9\\_15](https://doi.org/10.1007/978-3-642-23175-9_15).
- [8] D. Karrasch. “Comment on “A variational theory of hyperbolic Lagrangian coherent structures, Physica D 240 (2011) 574–598””. In: *Physica D: Nonlinear Phenomena* 241.17 (2012), pp. 1470–1473. ISSN: 0167-2789. DOI: <https://doi.org/10.1016/j.physd.2012.05.008>. URL: <https://www.sciencedirect.com/science/article/pii/S0167278912001443>.
- [9] P. Nolan, M. Serra, and S. Ross. “Finite-time Lyapunov exponents in the instantaneous limit and material transport”. In: *Nonlinear Dyn* 100 (2020), pp. 3825–3852.